Next Sustainability 6 (2025) 100102

Contents lists available at ScienceDirect

Next Sustainability

journal homepage: www.sciencedirect.com/journal/next-sustainability

Short communication

Electrochemical urea degradation and energy co-generation using palladium and iron-based catalysts

Nivaldo G. Pereira Filho, Victoria A. Maia, Rodrigo F.B. de Souza, Almir O. Neto *

Instituto de Pesquisas Energéticas e Nucleares, IPEN/CNEN-SP, 2242 Cidade Universitária, Av. Prof. Lineu Prestes, São Paulo, SP CEP 05508-900, Brazil

ARTICLE INFO

Keywords:
Pd electrocatalysts
Fe electrocatalysts
Urea Oxidation
Fuel Cell
Cyclic Voltammetry

ABSTRACT

Cyclic voltammetry and in-situ ATR-FTIR spectroscopy experiments revealed that urea oxidation occurs through both faradaic direct and indirect mechanisms. The Pd/C electrocatalyst facilitated the formation of formate and NO_x species, while Fe/C predominantly promoted formate formation via an indirect pathway, attributed to the high activity of iron in water activation. Polarization and power density curves indicated that both electrocatalysts degraded urea with simultaneous energy co-generation, showing comparable activity. Pd/C achieved a power density of 1.3 mW cm^{-2}, while Fe/C reached 1.1 mW cm^{-2}. Although Pd/C demonstrated advantages in reaction kinetics, the significantly lower cost of iron positions Fe/C as a promising alternative for practical applications, particularly in direct urea-fed fuel cell reactors. Additionally, Fe/C exhibited 50 % higher urea consumption near the open circuit potential compared to Pd/C, highlighting its potential for the development of more cost-effective and efficient fuel cell designs.

1. Introduction

Nitrogen is an essential resource due to its role in protein synthesis and industrial production. However, the increasing demand for nitrogen compounds has significantly altered the global nitrogen cycle, leading to the introduction of various reactive nitrogen species into the environment, such as NO_x, ammonia, and urea [1]. This alteration in biogeochemical nitrogen flows has resulted in serious environmental issues, including the continuous deterioration of air quality, eutrophication, and other water quality problems [2,3]. Consequently, the effective management of reactive nitrogen in global systems has become crucial for reducing pollution and achieving sustainable development goals.

Urea, a metabolic molecule present in all living organisms, plays a significant role in many biological processes. It is the most abundant nitrogen carrier in human excrement and the dominant source of nitrogen in domestic wastewater [4]. Despite its relatively low toxicity, there is growing concern that excessive urea loads in wastewater are contributing to the eutrophication of surface waters, particularly in sensitive coastal areas [5].

To address this issue, various research groups are exploring methods to reduce urea levels in wastewater. Among the approaches studied are adsorption and phase-transfer methods [5], biological nitrogen removal processes (with hydraulic retention times of up to several days) [6], and electrochemical treatments, which offer relatively fast urea degradation rates (with retention times within a few hours). Electrochemical treatment presents advantages such as operational flexibility and potential for energy sustainability. Electrochemical systems have explored mixed metal oxide anodes based on RuO_2, IrO_2, and PtO_2 for treating low-concentration urea solutions [4,7–9].

However, it is important to recognize that urea-containing wastewater is an underutilized resource, with significant chemical energy and hydrogen content that could be harnessed. Under strong oxidation conditions, the urea molecules in wastewater can be converted into mineralized products (N_2, CO_2), while simultaneously recovering the energy contained in the chemical bonds. In this context, the urea oxidation reaction (UOR) has been proposed as a promising route for energy generation in fuel cell-type devices [10,11].

The UOR has been studied using fuel cell anode catalysts based on Ru, Pt, and Au [12,13]. However, recent advances suggest that nickel may offer significant improvements due to its high stability, abundance, and low cost [14]. Beyond nickel, other materials have shown promising potential, such as iron, where the transition from Fe^{2+} to Fe^{3+} occurs at a less positive potential than nickel, suggesting it may exhibit superior catalytic activity for UOR. In alkaline solutions, under the influence of an anodic potential, most iron compounds form a hydrated oxide layer. These surface hydrated oxides demonstrate better electrochemical

* Corresponding author.
E-mail address: aolivei@usp.br (A.O. Neto).

https://doi.org/10.1016/j.nxsust.2025.100102
Received 3 October 2024; Received in revised form 3 January 2025; Accepted 6 January 2025
Available online 15 January 2025

activity than pure FeOOH, mitigating the limitations imposed by the poor conductivity of FeOOH [15]. Palladium, more abundant than platinum in the Earth's crust, has also demonstrated superior efficacy in oxidizing other molecules for energy generation in alkaline media [16–18]. The electrochemical oxidation of urea, especially in fuel cells, presents itself as a promising solution, offering not only pollutant degradation but also the possibility of co-generating electrical energy. This study investigated the use of a fuel cell as a flow reactor for urea degradation, employing Pd/C and Fe/C as catalysts for the anode. These electrocatalysts were synthesized through sodium borohydride reduction and evaluated via cyclic voltammetry and in direct urea fuel cells. This study is significant as it explores the performance of these catalysts in urea oxidation, a process crucial for developing efficient and cost-effective energy storage and conversion technologies. The findings could contribute to advancements in fuel cell technology and offer insights into optimizing electrocatalysts for practical applications.

2. Experimental

Pd/C and Fe/C catalysts were synthesized using a borohydride reduction method, incorporating 20 % by mass of the metal and 80 % of Vulcan XC 72 carbon as the support. Palladium(II) nitrate ($Pd(NO_3)_2{\cdot}2\,H_2O$ – Aldrich) and iron(II) chloride tetrahydrate ($FeCl_2{\cdot}4\,H_2O$ - Sigma) served as the metal precursors. In the preparation process, the support and metal precursors were dissolved in a 50/50 (v/v) mixture of water and 2-propanol. Sodium borohydride was then added in excess, along with 10 mL of 0.01 M KOH. The resulting catalysts were washed with water, dried at 70°C for 2 hours, and vacuum-filtered to obtain the final product.

Transmission electron microscopy (TEM) was performed using a JEOL JEM-2100 microscope operating at 200 keV. To analyze the size distribution of nanoparticles, histograms were constructed based on measurements from 300 particles for each electrocatalyst. X-ray diffraction (XRD) analysis was conducted using a Rigaku Miniflex II diffractometer with a CuKα radiation source (wavelength 1.5406 Å). The diffraction patterns were recorded over a 2θ range of 20° to 90° with a scanning rate of 2° per minute.

Electrochemical investigations were carried out using a three-electrode setup with a PGSTAT 302 N potentiostat/galvanostat (Metrohm Autolab). The working electrode was constructed by applying an ultrathin, porous layer of the catalytic material onto a vitreous carbon substrate. This catalytic layer was prepared by creating a colloidal suspension containing 8 mg of the catalytic precursor, 600 μL of high-purity water, 400 μL of anhydrous isopropanol (99.9 % purity), and 15 μL of Nafion® D-520. The suspension was sonicated to ensure homogeneity. An Ag/AgCl electrode (3.0 mol L^{-1} KCl) was used as the reference electrode, while a platinum plate electrode (surface area: 2 cm^2) served as the counter electrode. The electrochemical cell was filled with a 1.0 mol L^{-1} NaOH electrolyte solution. Electrochemical measurements were performed using cyclic voltammetry with a scan rate of 10 mV s^{-1}, within a potential window of −0.85 V to + 0.30 V (vs. Ag/AgCl reference electrode). Voltammetric data were obtained under two different experimental conditions: with and without the presence of urea. Spectro-electrochemical ATR-FTIR in situ measurements were performed with a Nicolet 6700 FT-IR spectrometer equipped with an MCT detector cooled with liquid N_2 and an ATR accessory (MIRacle with a Diamond/ZnSe Crystal Plate Pike®).

Direct urea fuel cells were tested using Pd/C and Fe/C electrocatalysts as the anode materials and Pt/C electrocatalysts as the cathode material. The cell configuration featured a carbon-cloth electrode substrate treated with Teflon and a Nafion® 117 membrane as the electrolyte. The anode and cathode electrodes were thermally bonded to either side of the Nafion® 117 membrane at 398 K (125°C) for 300 seconds under a pressure of 22 MPa (225 kgf cm^{-2}). Each anode electrode was loaded with 1.0 mg cm^{-2} of catalytic material (Pd or Fe), while the cathode was loaded with 1.0 mg cm^{-2} of Pt.

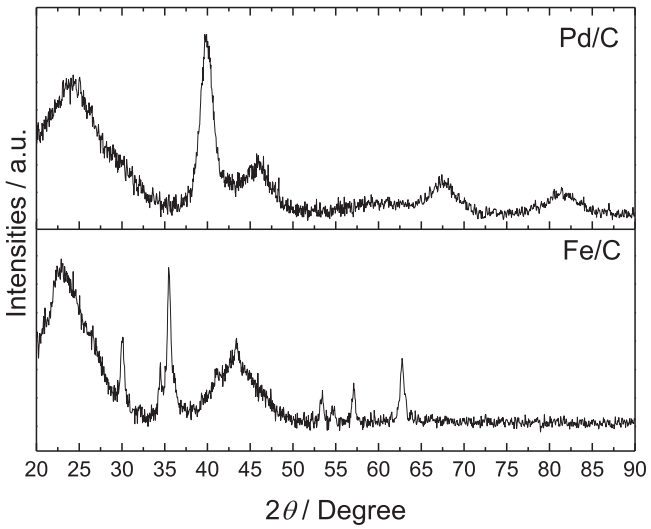

Fig. 1. X-ray diffractograms of Pd/C and Fe/C electrocatalysts prepared via sodium borohydride reduction for 2θ from up to 20∘ to 90∘.

Urea solution (0.33 mol L^{-1}) was introduced at a flow rate of approximately 1.0 mL min^{-1} , and the oxygen flow rate was maintained at 200 mL min^{-1} . Polarization curves were recorded at room temperature with 1.0 M urea and 1.0 M NaOH using a PGSTAT 302 N potentiostat/galvanostat (Autolab®) to evaluate the electrochemical performance of the fuel cell. For urea degradation experiments, chronoamperometry was conducted at potentials ranging from 0.3 V to 0.0 V. Samples were injected into a YL9100 Plus HPLC system (Young Lin Instrument, Korea). Separation was performed using a Luna C18 column (250 × 4.6 mm, Phenomenex, USA) in reverse phase, with UV-Vis detection at 210 nm. The mobile phase consisted of an isocratic run 100 % DI H_2O, at a flow rate of 0.5 mL min^{-1} and a temperature of 40°C. The urea calibration curve was determined to be $I = 52.67 \times [urea] + 1.24$, with $R^2 = 0.928$.

3. Results and discussions

Fig. 1 shows the XRD patterns for Pd/C and Fe/C electrocatalysts, both synthesized via sodium borohydride reduction, within the 2θ range of 20° to 90°. For the Pd structure, distinct diffraction peaks are observed at approximately 2θ ≈ 40º, 46º, 67º, 82º, and 86º, aligning with the reference pattern (JCPDS # 89–4897). The carbon support is identified by a peak near 25º, consistent with the reference JCPDS # 50–926. For the Fe/C material, a combination of Fe_3O_4 (JCPDS # 75–1609) and Fe_2O_3 (JCPDS # 2–1165) phases is detected. The Fe_3O_4 phase presents more intense peaks, with diffraction angles centered at ~30.2º, 34.8º, 43.2º, 53.5º, 57.2º, and 62.5º, while Fe_2O_3 peaks are observed around ~36º, 41.1º, and 54.3º.

Fig. 2 presents the TEM micrographs along with the corresponding particle size distribution histograms for the Pd/C and Fe/C electrocatalysts. The nanoparticles of both Pd/C and Fe/C are visibly clustered on the carbon support. Additionally, both electrocatalysts show a broad particle size distribution, with average particle sizes of 11 nm for palladium and 27 nm for iron. These results align with previous literature on electrocatalysts synthesized through sodium borohydride reduction [19,20].

Fig. 3a presents the cyclic voltammograms of the Pd/C and Fe/C electrocatalysts in the absence and presence of urea in solution. In the voltammogram of Pd/C without urea, the typical profile of polycrystalline palladium is observed, with the hydrogen adsorption and desorption region between −0.85 and −0.6 V, and the Pd oxidation and reduction peaks between −0.2 and −0.3 V [20]. Upon the introduction of urea into the solution, the hydrogen desorption peaks become more

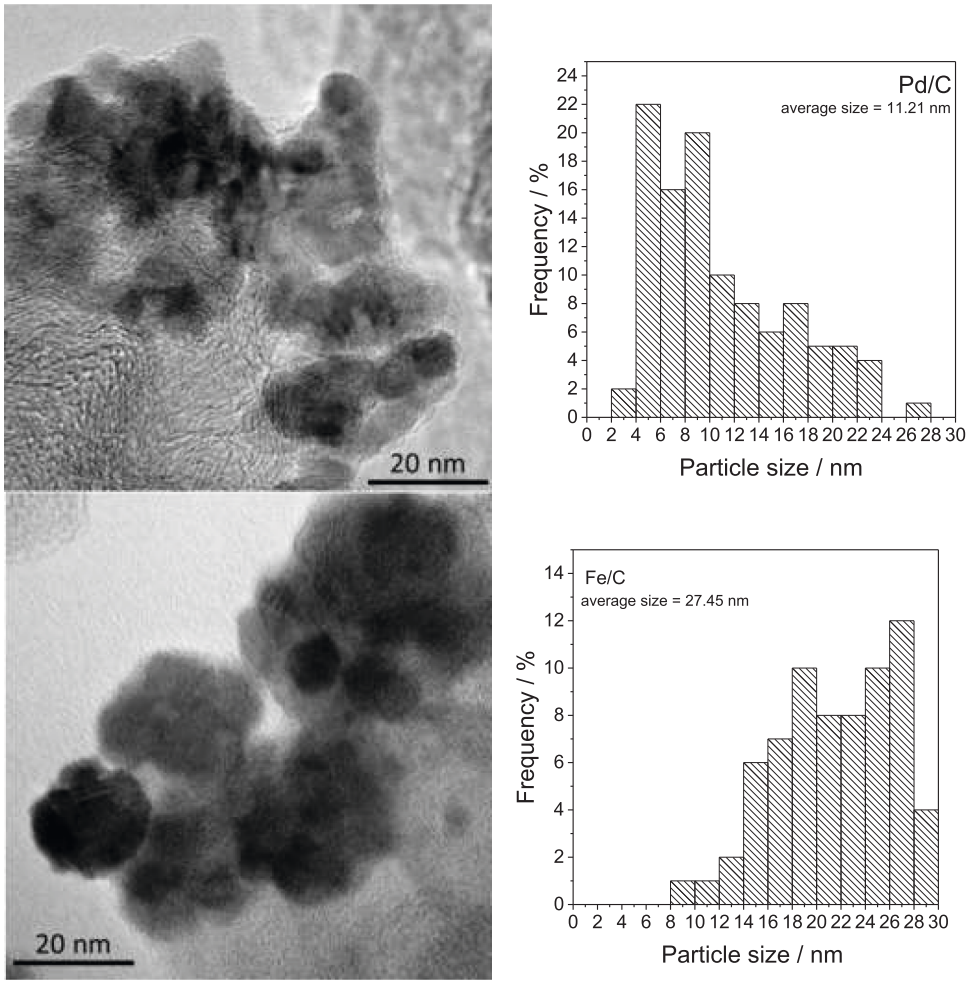

Fig. 2. Micrographs obtained by TEM and distribution histograms of Pd/C and Fe/C.

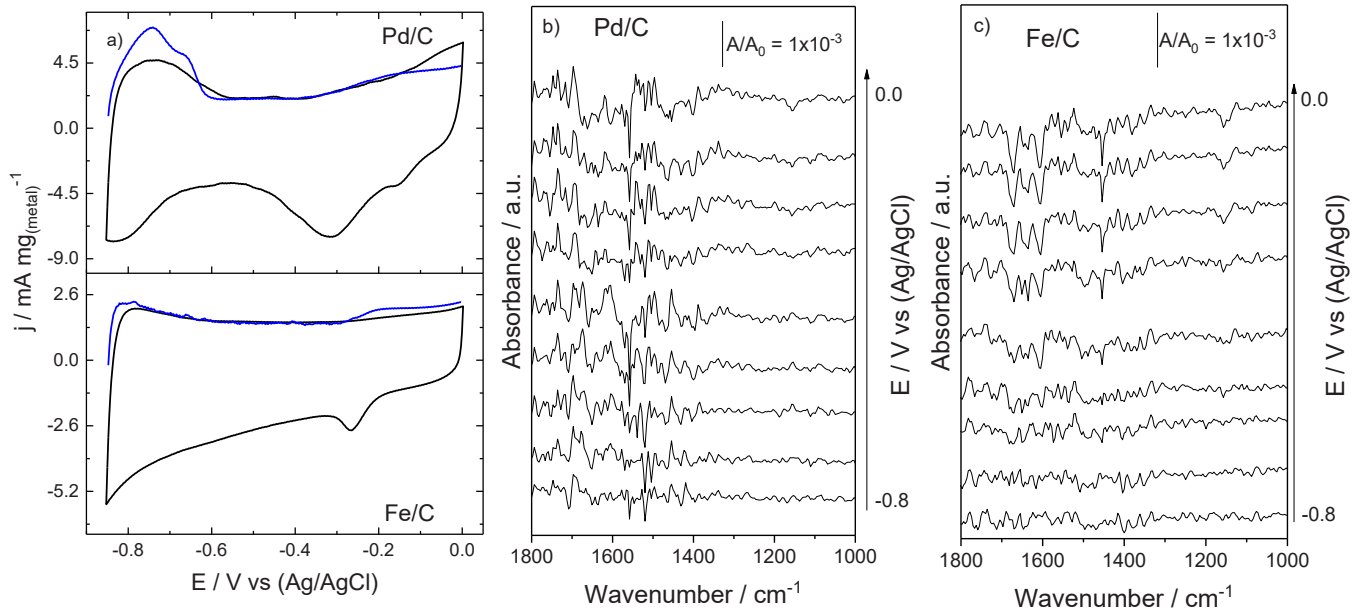

Fig. 3. a) Cyclic voltammetry in 1.0 mol L^{-1} of NaOH in black, 1.0 mol L^{-1} of NaOH + 0.33 mol L^{-1} urea in blue for Pd/C and Fe/C electrocatalysts, V = 10 mV/s; b) in-situ ATR-FTIR spectra collected on Pd/C; c) in-situ ATR-FTIR spectra collected on Fe/C in both spectra 1.0 mol L^{-1} of NaOH + 0.33 mol L^{-1} urea solution was used.

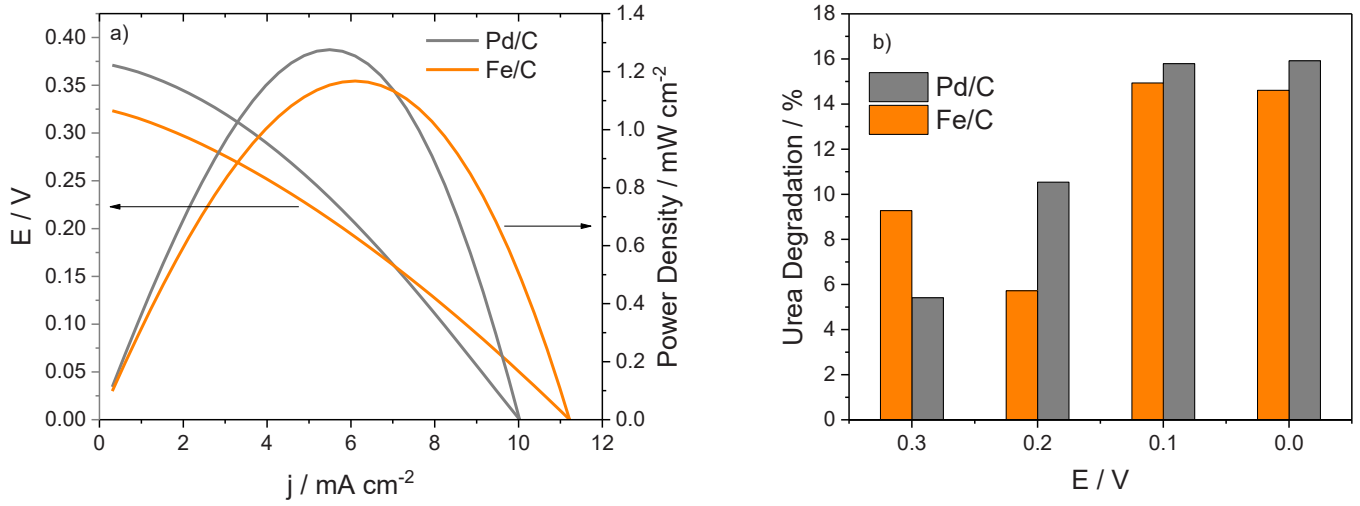

Fig. 4. Direct urea fuel cell experiments for Pd/C and Fe/C Flow = 1.0 mL min^{-1} of a 1.0 mol solution of KOH in the presence of 0.33 mol L^{-1} of urea. The cathode was maintained under an oxygen flow of 150 mL min^{-1}. Cell operating room temperature. Humidifier bottle temperature = 85 ∘C.

defined, while the oxidation current, which begins at −0.35 V, remains constant from −0.2 V onwards. In contrast, for Fe/C without urea, only a reduction peak around −0.28 V is observed, corresponding to the reduction of Fe(III) to Fe(II) [21]. With the addition of urea, an oxidation current with an onset potential of approximately −0.33 V is detected, although no substantially higher current than that of Fe/C in NaOH alone is observed.

To understand the behavior of urea in solution during the electrocatalytic process, in-situ ATR-FTIR spectroscopy-assisted voltammetry experiments were conducted. In Fig. 3b, for the Pd/C electrocatalyst, bands centered at 1674, 1453, and 1157 cm^{-1} , corresponding to the δs (NH_2), νs(CN), and ρ(NH_2) [22] modes of urea, increase in intensity between −0.8 and −0.4 V, indicating the accumulation of these species on the electrode surface. In the spectra obtained between −0.3 V and 0.0 V, these bands show negative intensities, suggesting the consumption of the adsorbed species. Additionally, from −0.4 V onwards, a band appears at 1222 cm^{-1} [23], associated with the νas(NO_2) mode, indicating the formation of NOx species. Another band, centered at 1339 cm^{-1} and attributed to the formate species [19], emerges at potentials more positive than −0.5 V, with its intensity increasing in spectra recorded at potentials higher than −0.3 V. These findings suggest that the formation of formates and NOx occurs both directly, through the adsorption and oxidation of urea on the noble metal surface, and indirectly, likely due to water activation and the formation of reactive oxygen species, which oxidize intermediates in solution. This mechanism is similar to that described by Ramos et al. [24] for methane oxidation. For Fe/C, a different behavior is observed compared to Pd/C. The urea bands indicate consumption starting at −0.6 V, and formate formation beginning at −0.8 V, but no bands related to NOx were detected. This suggests a predominance of the indirect pathway, which is attributed to the high activity of iron in water activation [25]. In neither of the two materials were relative carbonate bands observed, which would serve as an indication of the formation of CO_2 in an alkaline medium.

Fig. 4a shows the polarization and power curves for urea degradation in a fuel cell-type reactor. The open circuit potential for the palladium electrocatalyst is 0.37 V, while for iron it is 0.33 V, indicating that both electrocatalysts exhibit comparable activity and that the process occurs spontaneously with the co-generation of electrical energy. The power density for the palladium electrocatalyst is 1.3 mW cm^{-2}, whereas for iron it is 1.1 mW cm^{-2}, showing only a minor difference. Given that iron is significantly less expensive than palladium, this suggests that non-noble metals could offer a more economical approach for direct urea-fed fuel cell experiments. However, cyclic voltammetry results highlight the beneficial effects of using noble metals.

In Fig. 4b, it is observed that urea consumption at potentials near the open circuit is approximately 50 % higher for Fe/C compared to Pd/C. At less positive potentials, the urea consumption is quite similar (∼6 %) at potentials of 0.1 and 0.0 V. These results indicate efficient urea consumption of ∼16 % in a flow reactor operating at 1.0 mL min^{-1} , with a solution residence time of 2.4 min in the reactor. These results indicate that the urea oxidation process can occur via an indirect mechanism, where the oxidation is mediated by the formation of free radicals that attack the urea molecule.

4. Conclusion

This study demonstrated the degradation of urea using a flow reactor-type fuel cell, highlighting the performance of both Pd/C and Fe/C electrocatalysts. The cyclic voltammetry and ATR-FTIR spectroscopy results indicate that urea oxidation occurs through both faradaic direct and indirect mechanisms, with the formation of formate and NOx species in the case of Pd/C, and predominantly formate formation via the indirect pathway in Fe/C, likely due to iron's high activity in water activation. The polarization and power density curves show that both electrocatalysts exhibit urea degradation with energy co-generation and comparable activity, with only a minor difference in power density, where palladium achieves 1.3 mW cm^{-2} and iron reaches 1.1 mW cm^{-2}. Although Pd/C offers some advantages in terms of reaction kinetics, the significantly lower cost of iron makes Fe/C a promising alternative for practical applications, especially in direct urea-fed fuel cell reactors. Furthermore, Fe/C demonstrated 50 % higher urea consumption near the open circuit potential compared to Pd/C, further emphasizing its potential in cost-effective fuel cell designs.

Declaration of Competing Interest

The authors declare that they have no known competing financial interests or personal relationships that could have appeared to influence the work reported in this paper.

Acknowledgment

We are grateful to CAPES, CNPq (350514/2023–2, 302709/2020–7), and FAPEAM (012/2021 – POSGRAFE) for financial support.

References

[1] X. Wang, J.-P. Li, Y. Duan, J. Li, H. Wang, X. Yang, M. Gong, Electrochemical urea oxidation in different environment: from mechanism to devices, ChemCatChem 14 (2022) e202101906, https://doi.org/10.1002/cctc.202101906.

[2] M.D.B. Watanabe, E. Ortega, Ecosystem services and biogeochemical cycles on a global scale: valuation of water, carbon and nitrogen processes, Environ. Sci. Policy 14 (2011) 594–604, https://doi.org/10.1016/j.envsci.2011.05.013.

[3] U. Hinrichsen, F. Wulff, Biogeochemical and physical controls of nitrogen fluxes in a highly dynamic marine ecosystem—model and network flow analysis of the Baltic Sea, Ecol. Model. 109 (1998) 165–191, https://doi.org/10.1016/S0304-3800(98)00051-9.

[4] K. Cho, M.R. Hoffmann, Urea degradation by electrochemically generated reactive chlorine species: products and reaction pathways, Environ. Sci. Technol. 48 (2014) 11504–11511, https://doi.org/10.1021/es5025405.

[5] D. Weerakoon, B. Bansal, L.P. Padhye, A. Rachmani, L. James Wright, G. Silyn Roberts, S. Baroutian, A critical review on current urea removal technologies from water: an approach for pollution prevention and resource recovery, Sep. Purif. Technol. 314 (2023) 123652, https://doi.org/10.1016/j.seppur.2023.123652.

[6] M. Maurer, W. Pronk, T.A. Larsen, Treatment processes for source-separated urine, Water Res. 40 (2006) 3151–3166, https://doi.org/10.1016/j.watres.2006.07.012.

[7] W. Simka, J. Piotrowski, A. Robak, G. Nawrat, Electrochemical treatment of aqueous solutions containing urea, J. Appl. Electrochem. 39 (2009) 1137–1143, https://doi.org/10.1007/s10800-008-9771-4.

[8] B.J. Hernlem, Electrolytic destruction of urea in dilute chloride solution using DSA electrodes in a recycled batch cell, Water Res. 39 (2005) 2245–2252, https://doi.org/10.1016/j.watres.2005.04.018.

[9] W. Simka, J. Piotrowski, G. Nawrat, Influence of anode material on electrochemical decomposition of urea, Electrochim. Acta 52 (2007) 5696–5703, https://doi.org/10.1016/j.electacta.2006.12.017.

[10] V.S. Protsenko, Thermodynamic aspects of urea oxidation reaction in the context of hydrogen production by electrolysis, Int. J. Hydrog. Energy 48 (2023) 24207–24211, https://doi.org/10.1016/j.ijhydene.2023.03.295.

[11] I.L. Lera, S. Khasnabis, L.M. Wangatia, O.E. Femi, P.C. Ramamurthy, An innovative catalyst of PdNiP nanosphere deposited PEDOT:PSS/rGO hybrid material as an efficient electrocatalyst for alkaline urea oxidation, Polym. Bull. 80 (2023) 1265–1283, https://doi.org/10.1007/s00289-022-04100-w.

[12] W. Xu, Z. Wu, S. Tao, Urea-based fuel cells and electrocatalysts for urea oxidation, Energy Technol. 4 (2016) 1329–1337, https://doi.org/10.1002/ente.201600185.

[13] J. Miao, Q.-L. Hong, P. Zhang, Z.-F. Ren, A.-C. Zhao, Y.-H. Li, P.-F. Wang, Y. Chen, Self-supported Pt nanoparticles-NiFeP nanosheets arrays nanohybrid with hydrophilic surface towards urea electrolysis, Appl. Surf. Sci. 652 (2024) 159276, https://doi.org/10.1016/j.apsusc.2023.159276.

[14] W. Shi, R. Ding, X. Li, Q. Xu, E. Liu, Enhanced performance and electrocatalytic kinetics of Ni-Mo/graphene nanocatalysts towards alkaline urea oxidation reaction, Electrochim. Acta 242 (2017) 247–259, https://doi.org/10.1016/j.electacta.2017.05.002.

[15] H.A. Bandal, H. Kim, In situ construction of Fe3O4@FeOOH for efficient electrocatalytic urea oxidation, J. Colloid Interface Sci. 627 (2022) 1030–1038, https://doi.org/10.1016/j.jcis.2022.07.104.

[16] E.H. Fontes, C.E.D. Ramos, C.A. Ottoni, R.F.B. de Souza, E. Antolini, A.O. Neto, Glycerol dehydrogenation steps on Au/C surface in alkaline medium: an in-situ ATR-FTIR approach, Renew. Energy 167 (2021) 954–959, https://doi.org/10.1016/j.renene.2020.12.026.

[17] J. Nandenha, C.E.D. Ramos, S.G. da Silva, R.F.B. de Souza, E.H. Fontes, C.A. Ottoni, A.O. Neto, Borohydride reduction method for PdIn/C electrocatalysts synthesis towards glycerol electrooxidation under alkaline condition, Electroanalysis 33 (2021) 1115–1120, https://doi.org/10.1002/elan.202060322.

[18] R.S. Henrique, R.F.B. De Souza, J.C.M. Silva, J.M.S. Ayoub, R.M. Piasentin, M. Linardi, E.V. Spinacé, M.C. Santos, A.O. Neto, Preparation of Pt/C-In2O3.SnO2 electrocatalysts by borohydride reduction process for ethanol electro-oxidation, Int. J. Electrochem. Sci. 7 (2012) 2036–2046, https://doi.org/10.1016/S1452-3981(23)13861-2.

[19] M.C.L. Santos, L.C. Nunes, L.M.G. Silva, A.S. Ramos, F.C. Fonseca, R.F.B. de Souza, A.O. Neto, Direct alkaline anion exchange membrane fuel cell to converting methane into methanol, ChemistrySelect 4 (2019) 11430–11434, https://doi.org/10.1002/slct.201902421.

[20] V.A. Maia, J. Nandenha, M.H. Gonçalves, R.F.B. de Souza, A.O. Neto, Methane to methanol conversion using proton-exchange membrane fuel cells and PdAu/antimony-doped tin oxide nanomaterials, Methane (2023) 252–264.

[21] Z. Zeng, L. Yi, J. He, Q. Hu, Y. Liao, Y. Wang, W. Luo, M. Pan, Hierarchically porous carbon with pentagon defects as highly efficient catalyst for oxygen reduction and oxygen evolution reactions, J. Mater. Sci. 55 (2020) 4780–4791, https://doi.org/10.1007/s10853-019-04327-5.

[22] J. Grdadolnik, Y. Maréchal, Urea and urea–water solutions—an infrared study, J. Mol. Struct. 615 (2002) 177–189, https://doi.org/10.1016/S0022-2860(02)00214-4.

[23] L. Lietti, M. Daturi, V. Blasin-Aubé, G. Ghiotti, F. Prinetto, P. Forzatti, Relevance of the nitrite route in the NO adsorption mechanism over Pt–Ba/Al2O3 NO storage reduction catalysts investigated by using operando FTIR spectroscopy, ChemCatChem 4 (2012) 55–58, https://doi.org/10.1002/cctc.201100304.

[24] A.S. Ramos, M.C.L. Santos, C.M. Godoi, A. Oliveira Neto, R. Fernando B. De Souza, Obtaining C2 and C3 products from methane using Pd/C as anode in a solid fuel cell-type electrolyte reactor, ChemCatChem 12 (2020) 4517–4521, https://doi.org/10.1002/cctc.202000297.

[25] M. Okamura, M. Kondo, R. Kuga, Y. Kurashige, T. Yanai, S. Hayami, V.K. K. Praneeth, M. Yoshida, K. Yoneda, S. Kawata, S. Masaoka, A pentanuclear iron catalyst designed for water oxidation, Nature 530 (2016) 465–468, https://doi.org/10.1038/nature16529.